Chapter 3

Diurnal ozone cycle in the tropical and subtropical marine boundary layer

Abstract

A conceptual analysis of diurnal ozone (O_3) changes in the marine boundary layer (MBL) is presented. Such changes are most pronounced downwind of O_3 sources in tropical and subtropical latitudes, and during summer at higher latitudes. Previously, it has been assumed that daytime photochemical O_3 loss, and nighttime replenishment through entrainment from the relatively O_3-rich free troposphere, explains the diurnal O_3 cycle. We show, however, that in a net O_3-destruction environment (low NO_x) this diurnal cycle can be explained by photochemistry and advection, which establish a horizontal O_3 gradient that is typical for the MBL. We support this hypothesis firstly by calculations with a conceptual 1-D advection-diffusion model, and secondly by simulations with an interactive 3-D chemistry-transport model. The results are in good agreement with observations, for example, in the Indian Ocean Experiment (INDOEX).

1

3.1   Introduction

Since the recognition of ozone as an important chemical specie in the troposphere it has been extensively measured and monitored during campaigns and from ground stations. Some of these campaigns have been performed over the remote oceans, and a number of surface stations are situated in remote areas as well. These campaigns and surface stations were established to improve the knowledge about the "background" troposphere, i.e. the chemistry of unpolluted air. From these campaigns and stations it was discovered that the remote marine troposphere, especially in the tropics, is a significant sink region for many chemical species, including O_3 [e.g. Kley *et al.*, 1996]
It has long been recognized that, depending on the NO_x concentrations, two distinct O_3 regimes exist ($NO_x = NO + NO_2$). In areas with relatively high NO_x concentrations (NO_x exceeding roughly 50-100 pptv) O_3 production dominates destruction during daytime, while in low-NO_x environments (NO_x less than roughly 50-100 pptv) net O_3 destruction prevails [Crutzen, 1974]. The chemical lifetime of NO_x is only a few days, and both O_3 and NO_x have no oceanic source, so that most of the marine lower troposphere is a net O_3 destruction area. Indications of whether an area is a net O_3 source or a sink can be derived from the diurnal O_3 cycle, because photochemical production and destruction are restricted to daytime. A summary of such effects is given in Table 2. The table also shows the observed amplitude of the diurnal O_3 cycle, whether the amplitude is calculated from the daytime O_3 depletion rate or averaged over a longer period and the maximum observed O_3 concentration.

The amplitudes of the observed diurnal O_3 cycles have values of the order of a few ppbv. All campaigns observed that the maximum in the O_3 concentration over the oceans occurs late at night (just before sunrise) and that the minimum concentrations occur during the late afternoon (just before sunset). The depletion of O_3 under low-NOx conditions, mostly due to the photolysis of O_3 and the subsequent reaction of $O(^1D)$ with H_2O, causes the daytime O_3 decrease. After sunset O_3 starts increasing until sunrise. The increase in O_3 has been attributed to entrainment of relatively O_3-rich air from the free troposphere into the marine boundary layer (MBL). This has been confirmed by photochemical box models, budget studies and 1-D models in which this exchange was included (Table 1).

Reference	Model type	Entrainment rate (mm s^{-1})	Amplitude of diurnal O_3 cycle (ppbv)
Thompson and Lenschow (1984)	1-D	3	1
Paluch *et al.* (1995)	Box		0.75-2.25
Noone *et al.* (1996)	Budget	7	1
Heikes *et al.* (1996)	Budget	7	1
Ayers *et al.* (1997)	Box	3	0.5
Bremaud *et al.* (1998)	Box	1 (day) 14 (night)	< 0.5 2

Table 1. Diurnal O_3 cycle computations from several studies and inferred entrainment rates

Reference	Type of measure-ment	Location	Amplitude of diurnal O_3 cycle (ppbv)	Maximum O_3 concentration measured (ppbv)	Type of measure-ment data[a]
Oltmans (1981)	Surface Stations	Mauna Loa	2	25	T
		Samoa	1	20	
Liu *et al.* (1983)	Ship	Eq. Pacific Ocean	1	20	D
Piotrowicz *et al.* (1989)	Ship	Eq. Atlantic Ocean	1.5	50	T
Johnson *et al.* (1990)	Ship	Eq. Indian Ocean Eq. Pacific Ocean	1	30	T
Thompson *et al.* (1993)	Ship	Eq. Pacific Ocean	0-1.15	22	T
Anderson *et al.* (1993)	Aircraft	Eq. Atlantic Ocean	4	50	D
Oltmans and Levy II (1994)	Surface stations	Bermuda Barbados	1 1.5		T
Paluch *et al.* (1994)	Aircraft	Eq. Pacific Ocean	1.5-4	40	D
Paluch *et al.* (1995)	Aircraft	Eq. Atlantic Ocean	2.75	20	D
Ayers *et al.* (1996), Ayers *et al.* (1992), Ayers *et al.* (1997), Monks *et al.* (1998)	Surface station	Cape Grim	1.4 (summer)	35	T
Bremaud *et al.* (1998)	Surface station	Reunion	2	30	T
Lal *et al.* (1998)	Ship	Eq. Indian Ocean	1.5	30[b]	T
This study	Surface station	Eq. Indian Ocean	1.5	40	T

Table 2: Measurements of the diurnal O_3 cycle in marine locations.

One problem with these models, however, is that the entrainment is parameterized because the models cannot resolve the entrainment process explicitly. A usual procedure is to use a constant entrainment flux, which is either calculated from flux measurements, or from the entrainment velocity and an O_3 concentration increment across the top of the boundary layer:

$$\text{Entrainment flux} = w_e \, \Delta O_3 \qquad (3.1)$$

in which w_e is the entrainment velocity and ΔO_3 is the O_3 increment [Lenschow *et al.*, 1982; Thompson and Lenschow, 1984]. In this approach the models are allowed to reach an equilibrium in which the daytime removal equals the nighttime recovery. These two processes then establish the diurnal O_3 cycle.

A more extensive expression for the entrainment of O_3 into the boundary layer, derived from thermodynamic equations, is given by Bremaud *et al.* [1997]:

---

[a] D is the daytime O_3 depletion rate, and T is the average total over a longer period
[b] Value valid for the oceanic regions. In coastal regions concentrations increased to 70 ppbv

$$\delta_{O_3} = \alpha \frac{H_0}{\rho C_p Z_i} + \frac{\Delta O_3}{\Delta \theta}$$

in which δO_3 is the enhancement of O_3 throughout the entire boundary layer, ΔO_3 is the O_3 increment at the top of the boundary layer, ρ is the air density, C_p is the heat capacity of air, H_0 is the surface sensible heat flux, $\Delta \theta$ is the strength of the temperature inversion and α is a constant which expresses the ratio between the entrainment sensible heat flux and the surface sensible heat flux. The term δO_3 can be interpreted as the amount of O_3 transported into the boundary layer and distributed throughout the column per unit of time. In Table 3 some typical values for the above mentioned variables are summarized.

ΔO_3	-30 to 40 ppbv
H_0	10-100 Wm^{-2}
Z_i	500-1500 m
$\Delta \theta$	0.5-3 K

Table 3. Typical ranges of values used in equation (3.2). ΔO_3 is the O_3 increment at the top of the boundary layer, H_0 is the surface sensible heat flux, Z_i is the boundary layer height and $\Delta \theta$ is the strength of the temperature inversion.

With $\rho C_p = 1.3 \ 10^3 \ Jm^{-3}K^{-1}$ and $\alpha = 0.2$, the value of δO_3 can range between -6.6 and 8.8 ppbv hour^{-1} throughout the boundary layer, assuming ΔO_3 ranges between -30 to 40 ppbv [Kawa and Person, 1989; Paluch *et al.*, 1995; Noone *et al.*, 1996]. The boundary layer air can be replenished by free tropospheric air within a few hours according to this calculation, and O_3 concentration changes can be either positive or negative. The entrainment flux (δO_3) determines to a large extent the amplitude of the diurnal O_3 cycle. The enhancement fluxes derived from equation (2) are almost two orders of magnitude larger than what can be derived from Table 2. However, the values given in Table 2 are averages over longer periods of time, and the amplitude of the diurnal cycle on a given day can be 3 or 4 times larger than the average amplitude (see for example figures 3a and 3b). A rather high amplitude of 10 ppbv day^{-1} requires an enhancement flux of about 0.8 ppbv hour^{-1}, which is still an order of magnitude smaller than the values derived above, and an amplitude of 10 ppbv day^{-1} in the diurnal O_3 cycle in the MBL has rarely been observed. It can also be seen from equation (2) that the entrainment rate is strongly dependent on the strength of the inversion and the concentration increment over the inversion. It is therefore not very likely that the entrainment flux is constant, especially since numerous campaigns have shown that a wide range of ΔO_3 values can occur, sometimes even in the same area [Kawa and Person, 1989; Paluch *et al.*, 1995; Noone *et al.*, 1996]. The uncertainties involved in these calculations show that the "entrainment" approach, as an explanation for the diurnal O_3 cycle in the MBL, can be questioned.

The "entrainment" approach also provides a conceptual problem. Observations (Table 2) and models (Table 1) show that the daytime net photochemical destruction is counterbalanced by a nighttime increase. In the "entrainment" approach the O_3

concentration increase is caused by transport of O_3 rich air from the free troposphere. Both observations and model results in Tables 1 and 2 refer to a fixed "Eulerian" frame. If, however, such an airmass were advected horizontally, and no net O_3 depletion would occur because of the balance between daytime net photochemical destruction and nighttime replenishment, downwind reduction of O_3 concentrations and horizontal O_3 gradients could not occur. This disagrees with numerous observations, which clearly indicate that horizontal O_3 gradients do exist in the MBL and that very low O_3 values occur regularly. The entrainment flux as an explanation of the observed diurnal O_3 cycle is therefore questionable.

In this study an alternative explanation for the diurnal O_3 cycle under low NO_x conditions will be presented. This approach can explain why O_3 gradients and low O_3 concentrations exist in some parts of the MBL. In section 2 the model will be described, and in section 3 model results will be compared with observations from an island site in the Indian Ocean. A conceptual model to explain the diurnal O_3 cycle will be presented in section 4. The results from a case study are presented in section 5, after which a discussion follows in section 6.

3.2   The ECHAM model

The General Circulation Model (GCM) used in this study is the 19 layer European Center Hamburg Model, version 4 (ECHAM4). In this study the T30 version of the model, with a horizontal resolution of about 3.75° x 3.75° and a time resolution of 1800 seconds, is used. The model uses a hybrid _-p coordinate system from the surface to 10 hPa. Average pressure levels relevant for the troposphere and lower stratosphere are 990, 970, 950, 900, 840, 760, 670, 580, 490, 400, 320, 250, 190, 140, 100 and 75 hPa, referring to approximate mid-layer altitudes of 0.03, 0.14, 0.38, 0.78, 1.4, 2.1, 3.1, 4.2, 5.6, 7.0, 8.6, 10.2, 11.9, 13.8, 15.9 and 18.0 km above the surface. Tracer transport is calculated using a semi-Lagrangian advection scheme [Rasch and Williamson, 1990]. Vertical transports are included through parameterizations of vertical diffusion and convection [Roeckner *et al.*, 1996; Tiedtke, 1989]. An elaborate description of ECHAM4 and the simulated climate can be found in Roeckner *et al.* [1995], Chen and Roeckner [1996], and Haskins *et al.* [1995]. In this study, ECHAM4 is coupled to a tropospheric chemistry model that considers background CH_4-CO-NO_x-HO_x chemistry, emissions of NO and CO, dry deposition of O_3, NO_2, HNO_3 and H_2O_2, and wet deposition of HNO_3 and H_2O_2. Concentration changes due to chemical reactions are calculated explicitly for all species by means of an Eulerian Backward Iterative (EBI) scheme. A detailed description and analysis of the coupled chemistry GCM is given in Roelofs and Lelieveld [1995, 1997].

The model considers a biomass-burning source for NO of 6 Tg N yr^{-1}, and for CO of 700 Tg CO yr^{-1}, distributed according to Hao and Liu [1994]. NO emissions from soils and from lightning play an important role in the tropical tropospheric O_3 budget. These sources in the model are 5.5 Tg N yr^{-1}, distributed according to Yienger and Levy [1995], and 5 Tg N yr^{-1} parameterized according to Price and Rind [1992], respectively. Further, the model considers global NO emissions from fossil fuel burning (21 Tg N yr^{-1}; Benkovitz *et al.* [1996]), and CO emissions from fossil fuel burning (450 Tg CO yr^{-1}),

vegetation (100 Tg CO yr^{-1}), formation from natural (280 Tg CO yr^{-1}) and antropogenic (300 Tg CO yr^{-1}) higher hydrocarbons, oceans (40 Tg CO yr^{-1}) and wildfires (30 Tg CO yr^{-1}). CO emissions are distributed according to Lelieveld and Van Dorland [1995]. The total NO and CO emissions considered in the model are 37.5 Tg NO yr^{-1} and 1900 Tg CO yr^{--1}, consistent with IPCC [1994]. In view of the relatively long lifetime of CH$_4$, the CH$_4$ surface concentrations are prescribed.

The parameterization for dry deposition of O$_3$, NO$_x$, and HNO$_3$ is described in Ganzeveld and Lelieveld [1995, 1998]. It derives aerodynamic and stomatal resistances directly from parameters calculated by ECHAM4. The wet scavenging of HNO$_3$ and H$_2$O$_2$ is calculated using the large scale and convective cloud and precipitation properties calculated on-line by the climate model as described in Roelofs and Lelieveld [1995, 1997]. Stratospheric O$_3$ concentrations are prescribed between 1 to 2 model layers above the tropopause up to 10 hPa, the top level of the GCM. Transports of O$_3$ across the tropopause depend directly on the air motions simulated by the GCM. The simulated tropopause is marked by a potential vorticity of 3.5·10^{-6} K m^2 kg^{-1} s^{-1} poleward of 20˚ latitude [Hoerling *et al.*, 1993], and by a -2 K km^{-1} temperature lapse rate equatorward of 20˚ latitude.

The model realistically represents the seasonal variability of the O$_3$ photochemical production and of O$_3$ transport from the stratosphere [Roelofs and Lelieveld, 1995, 1997]. Surface O$_3$ concentrations as measured in remote and relatively clean conditions are also reproduced, but the model appears to underestimate O$_3$ concentrations in some polluted regions due to the neglect of higher hydrocarbon chemistry [Roelofs *et al.*, 1997].

In this study the ECHAM4 model was relaxed towards ECMWF analysis (nudged) for two periods: 16 March 1995 - 31 April 1995 and 1 February 1998 - 1 April 1998, applying the method described by Jeuken *et al.* [1996] and De Laat *et al.* [1999]. For the period 16 March –31 March 1995 output was available every hour (every second model time step).

3.3   Measurements

As part of the Indian Ocean Experiment (INDOEX), an observatory was established at the island of Kaashidhoo on the Maldives. This site is situated at 4.965ºN and 73.466ºE, and continuous measurements of several chemical species (e.g. O$_3$ and CO), aerosols and radiation are performed since 1998. In this study we will take a closer look at the surface O$_3$ measurements performed during February-March 1998 when the First Field Phase (FFP) of the INDOEX campaign took place. Figure 1 shows the observed surface O$_3$ concentrations at Kaashidhoo and O$_3$ concentrations from the nudged ECHAM model at that site. The observations show that the O$_3$ concentrations range between roughly 15 and 30 ppbv with a superimposed diurnal cycle. The ECHAM model shows higher O$_3$ concentrations than observed, with an average difference of about 10 ppbv. De Laat *et al.* [1999] have discussed a similar offset over the Indian Ocean, based on shipborne O$_3$ measurements. The discrepancy is likely explained by (1) overestimation of O$_3$ formation by "artificial" NO$_x$ transport by instantaneous mixing of emissions in the coarse (3.75º) grid cells of the model, and (2) underestimation of O$_3$ destruction through heterogeneous activation of reactive halogens from sea salt in the MBL [Vogt *et al.*, 1996]
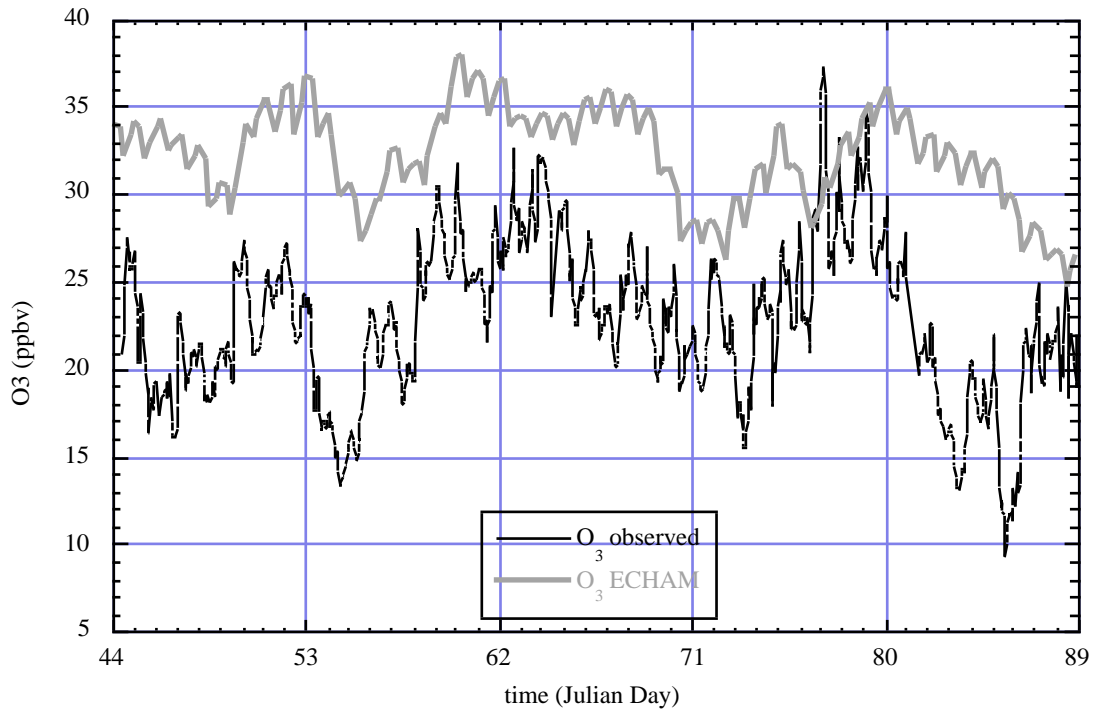
Figure 1: Observed and modeled O_3 concentrations during February and March 1998 at the Kaashidhoo surface observatory (4.965ºN and 73.466ºE) on the Maldives; O_3 concentrations in ppbv, time as Julian Days (JD 44.5 = February 13, 12:00 UTC).
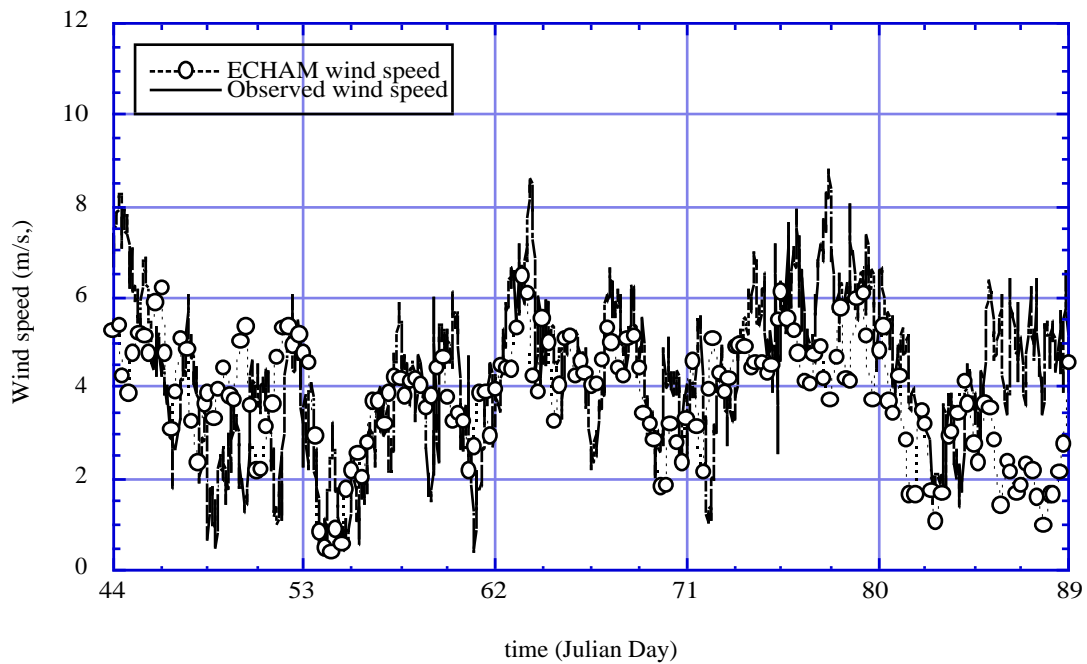

Figure 2: As Figure 1 but for the surface wind velocity.

The model reproduces the general tendencies, e.g. maxima in O_3 concentration around JD 53, between JD 58 and 70 and around JD 78 and minima around JD 48, 53 and 72. This is not surprising considering the fact that the modeled and observed surface-wind speeds (Figure 2) and wind directions (not shown) agree very well. The discrepancy between the observed temporal O_3 change and the modeled O_3 one between JD 80 and 88 are likely associated with differences between the observed and modeled wind speed and direction. In the model the winter monsoonal winds consistently originate from the northeast so that the airmasses travel over the southern tip of India and Sri Lanka towards Kaashidhoo. These areas are sources of O_3 precursors, thus counteracting the O_3 loss in the MBL. Therefore, the O_3 concentrations remain more or less constant. The observations, however, show west-northwesterly winds over this period, indicating a different origin of the airmass and thus a different chemical composition.

The diurnal O_3 cycles from both the observations and the model are shown in Figures 3a and 3b, where a running mean is calculated for both observations and model. Figures 3a and 3b show that the model produces a very similar diurnal O_3 cycle as seen in the observations, in spite of the ~ 10 ppbv offset in O_3 levels: a maximum concentration at the end of the night and a minimum concentration in the late afternoon. The model somewhat underestimates the amplitude of the diurnal cycle, although it should be considered that the model output was only available at 0, 6, 12, and 18 UTC, so that it is possible that not all the modeled peaks in O_3 are captured. The agreement between model and observations can be seen even better in Figure 4, which shows the daily averaged diurnal cycle from the running mean for both observations and model.
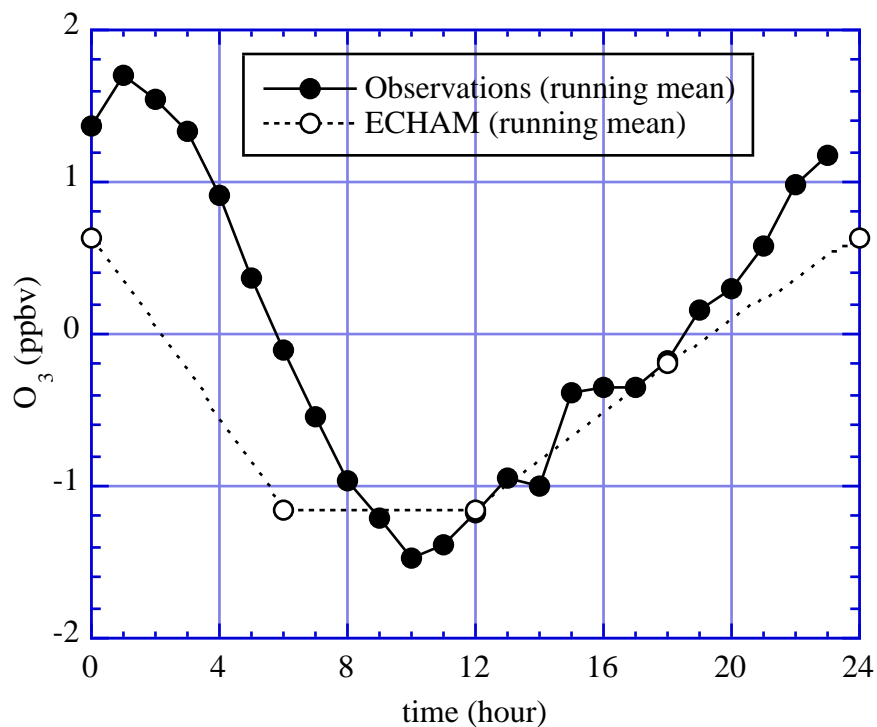

Figure 4: The averaged diurnal O_3 cycle for the period of 13 February to 1 April 1998, from the observations at the Kaashidhoo observatory and from the ECHAM model. Hours in UTC, local noon is at 07:00 UTC.
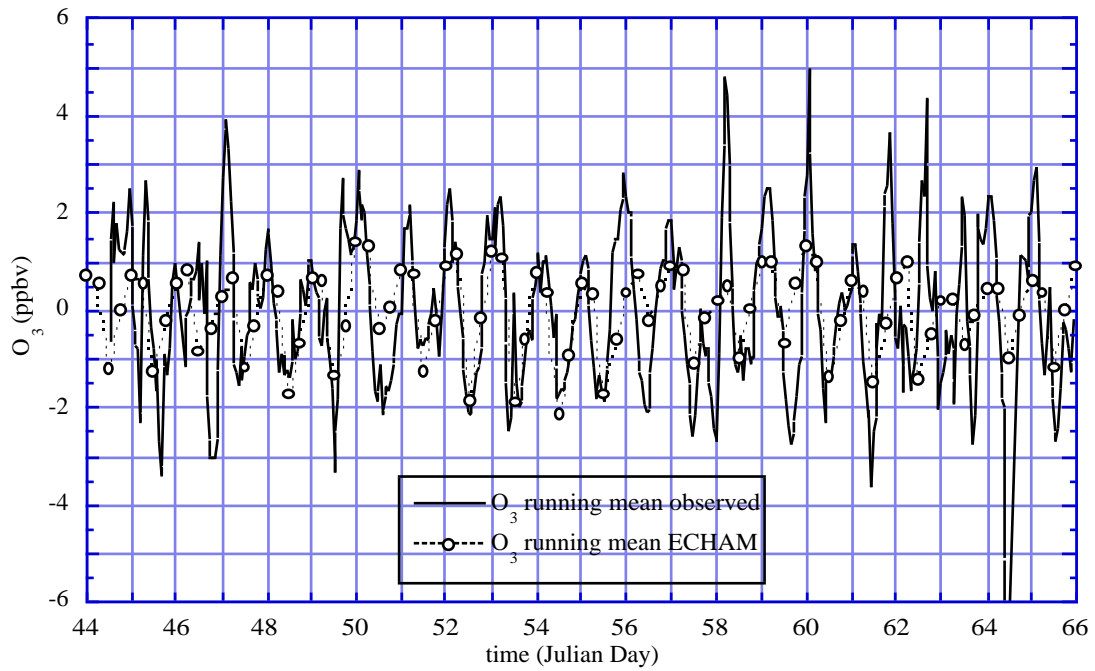
Figure 3a: Diurnal O$_3$ cycle as observed at Kaashidhoo and from the ECHAM model for the period 13 February to 7 March (JD 44 - 66) 1998. The figure shows the difference between the actual concentrations and a 24-hour running mean. Concentrations in ppbv.
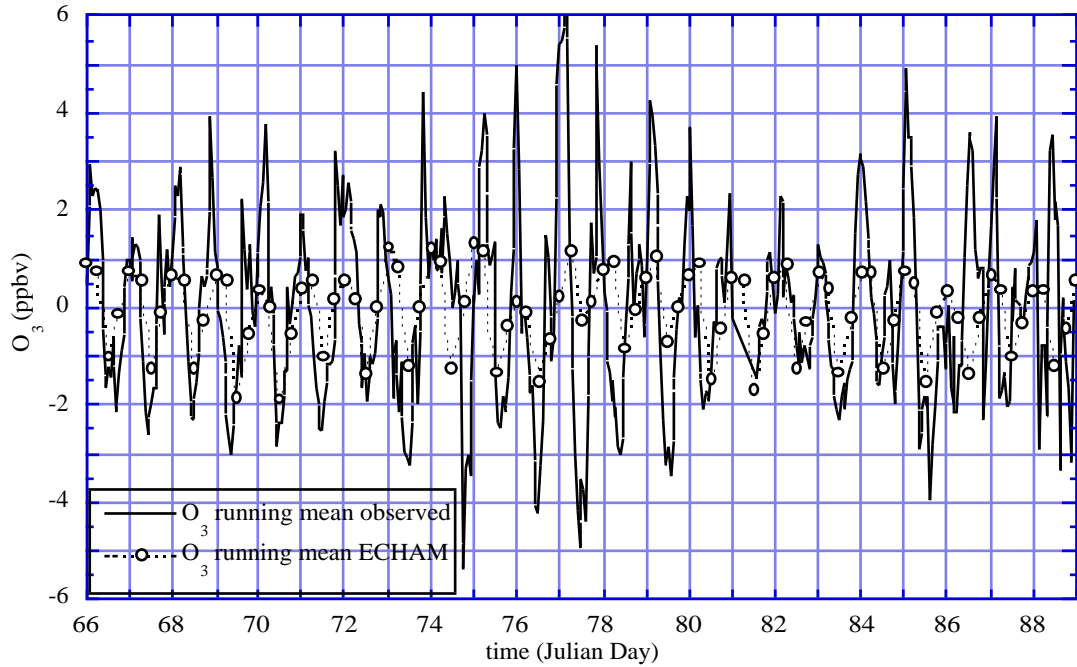

Figure 3b: As Figure 3a but for 7 March – 1 April (JD 66 - 89) 1998.

Considering that the ECHAM model has a vertical resolution of 19 layers, and the MBL is resolved by only 4 (5) layers (~ 30, 140, 380 and 780 (1480) meter altitude), the model is obviously not capable of resolving a small scale process like the entrainment of free tropospheric air into the MBL. The possibility of the vertical diffusion parameterization being responsible for entraining free tropospheric air, and thus the diurnal cycle of O_3 in the model, can be ruled out. Figure 5 shows the O_3 concentrations at the five lowest ECHAM model levels for the period 17-23 March 1995 at 5.559ºN, 61.875ºE. This grid point is situated at the central Arabian Sea, and the temporal O_3 changes are typical for the modeled tropical MBL. The O_3 concentrations in the three lowest layers (up to 380 m) are the same and show a very distinct diurnal cycle (local time of sunrise is approximately 03:00 UTC). These 3 layers represent the MBL in the model. If vertical diffusion would be responsible for the downward transport of O_3, it can be expected that during JD 76-78.5 a gradual decrease in O_3 would take place. Vertical mixing would bring air with lower O_3 concentrations into the boundary layer and O_3 would be photodissociated during daytime as well. Since such a gradual decrease is not discernable, the vertical diffusion can be assumed to be small. In fact, a small exchange between the MBL and the free troposphere is quite realistic. Due to the nearly constant surface temperatures over the ocean, the dynamics of the MBL are much the same during night and day (contrary to the continental boundary layer, which shows a distinct diurnal cycle). The height of the MBL changes only very slowly in time, it shows no diurnal cycle and has a well-defined inversion [Garratt, 1992]. If vertical transport can be ruled out as an explanation for the diurnal O_3 cycle in the model, the question remains what is responsible. Below we will show that this is solely caused by horizontal transport.
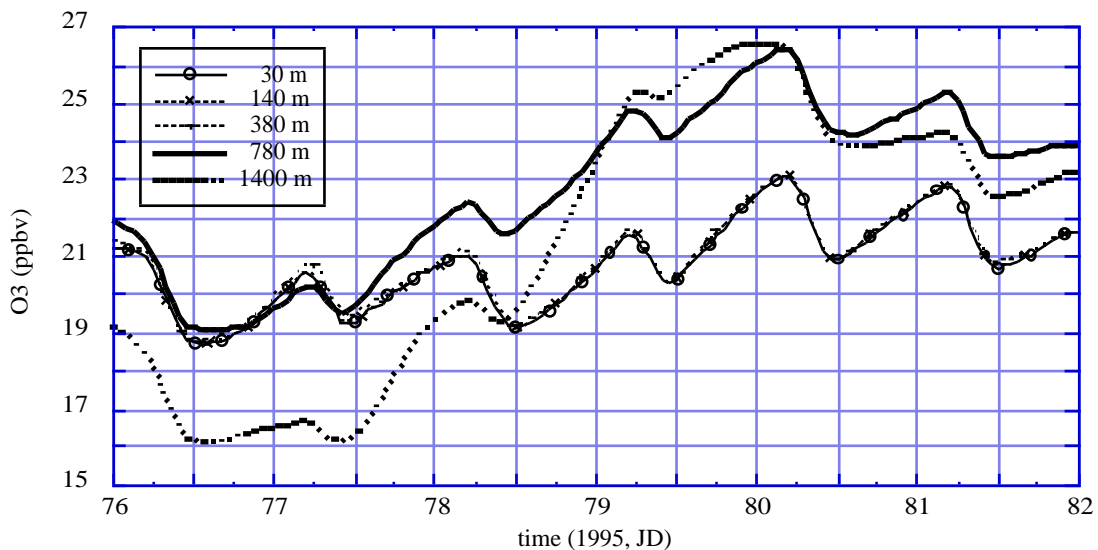

Figure 5: The modeled O_3 concentration for the grid point at 5.559ºN, 61.875ºE for the period of 17 – 23 March 1995 (JD 76 – 82) at the 5 lowest model levels. Hours in UTC, local noon is at 08:00 UTC.

3.4 1-Dimensional advection-diffusion equation

Consider an airmass being transported over sea in an NO_x-poor environment (lagrangian view). In the absence of vertical mixing, O_3 would remain constant during the night. During daytime O_3 would be depleted due to net photochemical destruction. Such a sequence will show up as step-wise changes in time: an O_3 decrease during the day and no change in O_3 concentration during the night [e.g. Sander and Crutzen, 1996]. Turbulence in the boundary layer will moderate the step-wise O_3 decrease to a more gradual profile. This has been observed regularly in the MBL [Johnson *et al.*, 1990; Lal *et al.*, 1998], and a typical meridional O_3 gradient over the Indian Ocean is 1.5 ppbv deg^{-1} [Lal *et al.*, 1998]. Suppose that the airmass is transported with an average wind speed of 4 ms^{-1} (Figure 2). The airmass will travel 170-175 km ($\approx$ 1.5 deg) in 12 hours. With an O_3 gradient of 1.5 ppbv deg^{-1} the O_3 level must be replenished by 2.25 ppbv during the 12 nighttime hours. Net photochemical destruction during daytime will then again lead to the depletion of O_3 so that the amplitude of the diurnal cycle is 1.125 ppbv for this example. According to Table 2, the observed amplitudes of the diurnal O_3 cycle agree well with this calculation. For an observer at a fixed point the O_3 changes would thus appear as a nighttime increase (transport) and daytime decrease (net photochemical loss).

The gradient causing the nighttime increase is directly related to the daytime depletion in O_3. A stronger decrease during the day would also lead to a larger horizontal O_3 gradient, and thus a sharper increase during the night. In this approach the daytime decrease will always be counteracted by the same nighttime increase. This hypothesis can be tested numerically by solving the 1-dimensional advection-diffusion equation:

$$\frac{\partial c}{\partial t} + u\frac{\partial c}{\partial x} - D\frac{\partial c}{\partial x^2} = 0 \qquad (3)$$

In which c is a tracer concentration, u is the average horizontal velocity and D is the diffusion coefficient. This equation describes the horizontal transport of a substance by the wind in the presence of horizontal diffusion. This is a good analogy for the horizontal transport of O_3, in which case diffusion is equivalent to boundary layer turbulence. The equation is solved with a Crank-Nicholson numerical scheme [Vreughdenhil, 1992]. The daytime depletion rate (amount of tracer depleted per second) is calculated as a $\cos^2$ function of time, and in such a manner that the total daytime depletion is roughly 3 concentration units. At night no depletion is assumed. The model was run with a time step of 600 seconds and during 2000 time steps. The horizontal grid distance was 2500 m and the number of grid points was 1000. The average horizontal velocity was chosen at 4 ms^{-1} and the tracer concentration at the boundary (x=0) was chosen at 20. It appears that the model reaches equilibrium within two days. Figure 6 shows the concentration as a function of the distance for two different values of the diffusion coefficient after equilibrium is reached. For a relatively low diffusion coefficient the profile shows the step-wise changes, while for a higher value of the diffusion coefficient the profile shows a constant gradient. Observations show that O_3 gradients are quite smooth [Johnson *et al.*, 1993; Lal *et al.*, 1998], so that a small diffusion coefficient is probably not realistic.
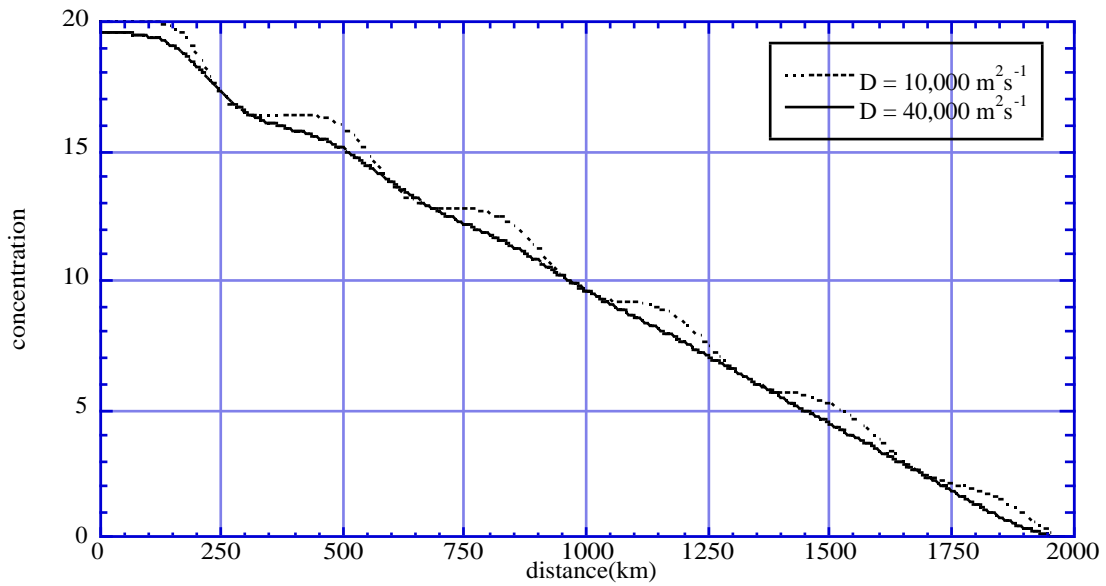
Figure 6: Tracer concentration calculated from the 1-dimensional advection-diffusion equation for two different values of the diffusion parameter.
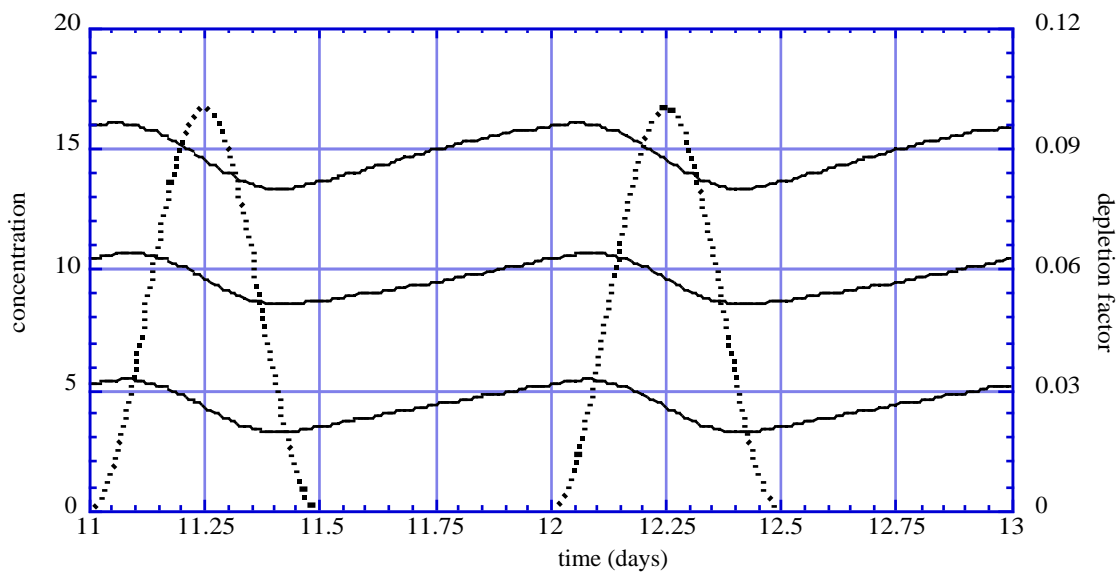

Figure 7: Concentration (arbitrary units) as a function of time for the solution of the 1-dimensional advection-diffusion equation with $D = 40,000$ m^{2}s^{-1}. From top to bottom the concentrations are plotted (solid lines) at distances of 500, 1000 and 1500 km respectively, and the dotted line shows the depletion factor.

Figure 7 shows the temporal concentration changes for D = 40,000 m^2s^{-1} for different fixed points. The lowest concentrations appear during late afternoon after the maximum depletion rate, as expected. The concentration at every grid point shows the same temporal behavior and the amplitude of the diurnal cycle is the same, because, in this example, the depletion rate is only a function of time and not of the concentration of the tracer. Figure 7 thus shows a sharp daytime decrease and a gradual nighttime increase. This feature has often been observed [Oltmans, 1981; Ayers *et al.*, 1997; Lal *et al.*, 1998] and can also be seen in the ECHAM model results (Figure 5).

The amount of photochemicaly destroyed O_3 is, however, dependent on the O_3 concentration itself. Numerical experiments in which the depletion rate is assumed to be dependent on the concentration indeed show that the amplitude of the diurnal cycle decreases with decreasing concentration, but the gradual increase in concentration during the night and the rapid daytime decrease remain unchanged. These experiments also lead to the conclusion that in a lagrangian time frame, i.e. travelling with the airmass, the temporal O_3 profile shows step-wise decreasing values. This can be seen in Figure 8, which shows the tracer concentration when travelling with the airmass.
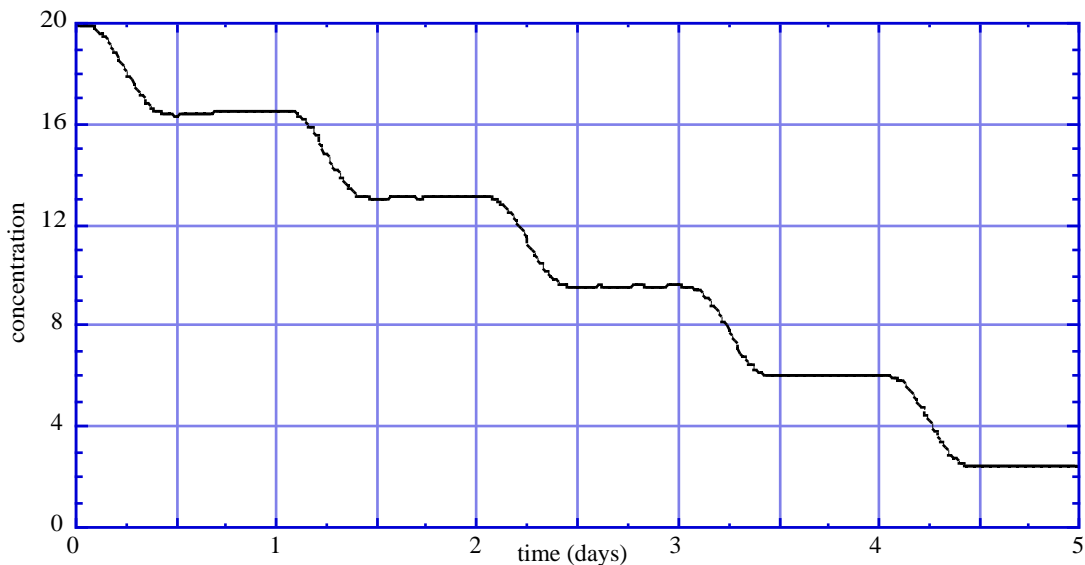

Figure 8: Concentration of a tracer calculated from the 1-dimensional advection-diffusion equation when travelling with the airmass (Lagrangian experiment).

3.5   Results from the ECHAM model

To compare the lagrangian conduct of O_3 in the ECHAM model with the 1-D advection-diffusion concept, a trajectory model was used to monitor the O_3 during transport. The trajectory model was applied to the 3-D ECHAM wind fields. The wind fields were updated every 6 hours. A fourth-order Runge-Kutta scheme was used to advect a set of points in 3-D space, and the wind velocities were linearly interpolated for the parcel in both space and time. The time step used for the trajectory calculations was
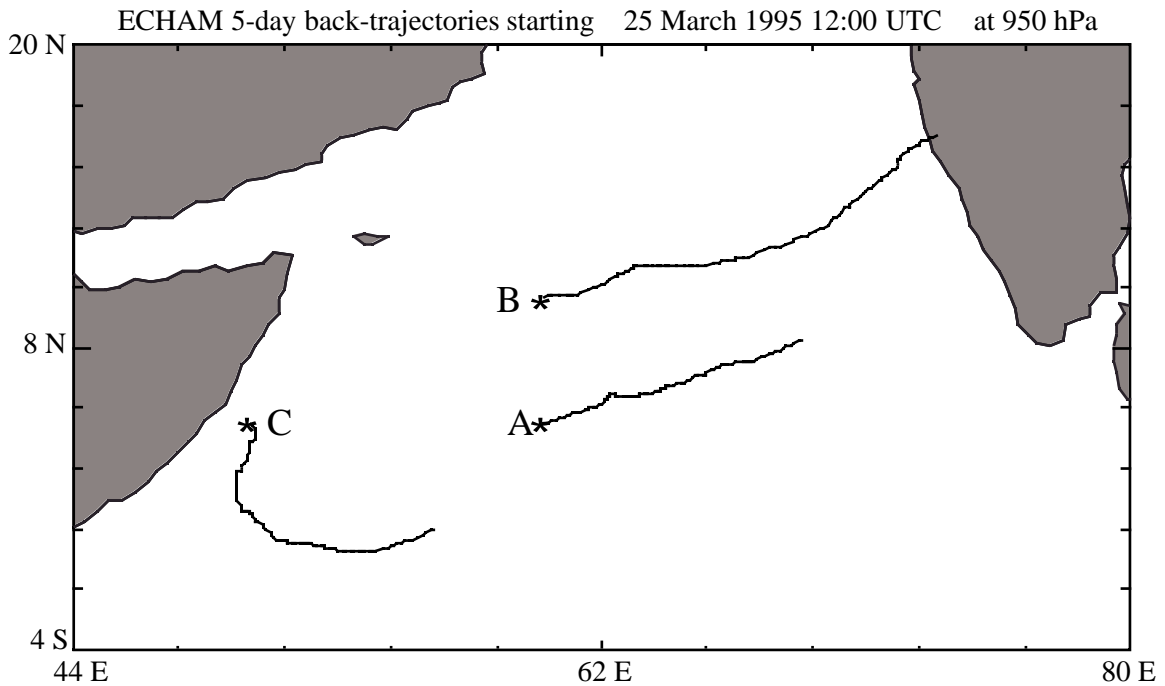
ECHAM 5-day back-trajectories starting   25 March 1995 12:00 UTC   at 950 hPa

Figure 9a: Horizontal position of three 5-day back-trajectories calculated from the ECHAM model output. Trajectories were started on 25 March 1995 at 12:00 UTC (JD 84.5), at an altitude of 950 hPa, at 60ºE, 5ºN (trajectory A), 60ºE, 10ºN (trajectory B) and 50ºE, 5ºN (trajectory C).
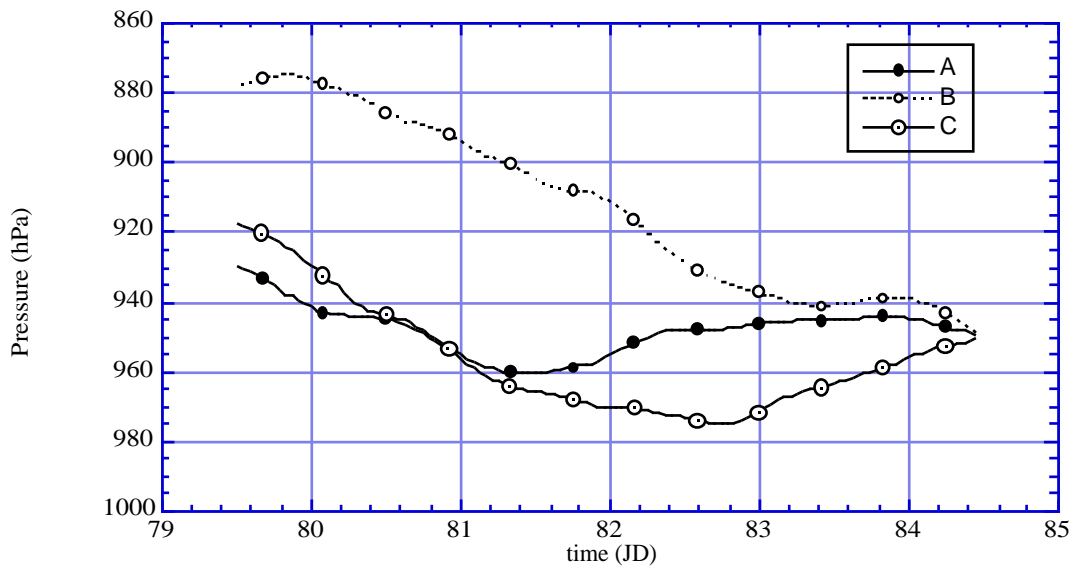
Figure 9b: Vertical displacements of the back-trajectories shown in Figure 9a.

30 minutes. Time and location of the trajectories were subsequently used to retrieve 1-hourly fields along the trajectories. Figure 9a shows the position of three 5-day back-trajectories starting on 25 March 1995 at 12:00 UTC at an altitude of 950 hPa. The trajectories A and B clearly follow the northeasterly flow over the Arabian Sea. Figure 9b shows the vertical displacements. The trajectories A and C remain in the lowest levels of the MBL most of the time, while trajectory C originates from a higher altitude, although still close to the top of the MBL.
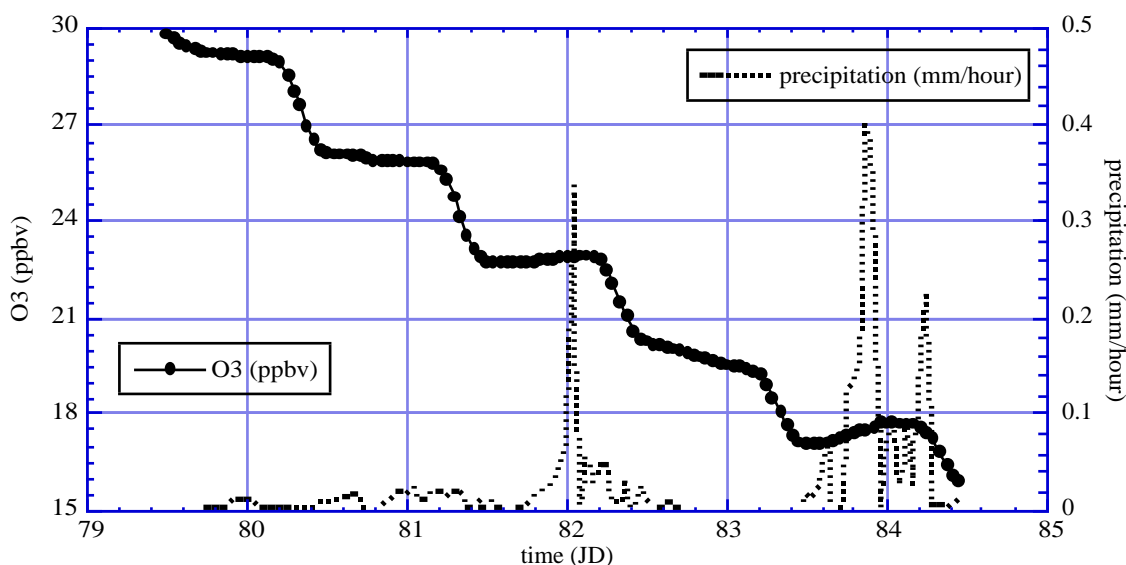

Figure 9c: O_3 concentrations and the precipitation rates along back-trajectory A, as calculated with the ECHAM model.

Figure 9c shows O_3 and the precipitation rate along trajectory A. The O_3 concentration shows the step-wise changes as predicted. Calculated NO_x concentrations varied between 24 and 40 pptv, which is in the net O_3 destruction regime. The small increases in O_3 around JD 82 and JD 84 are related to convective precipitation in the model. The precipitating clouds in the model are associated with mixing of boundary layer air with air from aloft which, in this case, had a higher O_3 concentration. This step-wise O_3 decrease is typical for model output in areas remote from NO_x sources, so that NO_x concentrations are well below the net O_3 production limit and the airmasses are subject to net O_3 loss at least a few days. In such cases almost all the O_3 increases along the trajectories are related to convection in the model [Lelieveld and Crutzen, 1994].

Figure 9d shows the concentrations of O_3 and NO_x along trajectory B. Again, the step-wise changes in O_3 are evident. As can bee seen in Figure 9a, this trajectory starts close to the Indian subcontinent where pollutants are emitted. This explains the relatively high NO_x concentrations at the start of the trajectory. The rates of O_3 changes in this case are different compared to trajectory A. Between JD 79.5 and 81.5 the net O_3 destruction is small. The concentrations of NO_x are close to the net O_3 production limit so that relatively little O_3 is lost during daytime compared to the total O_3 concentrations.
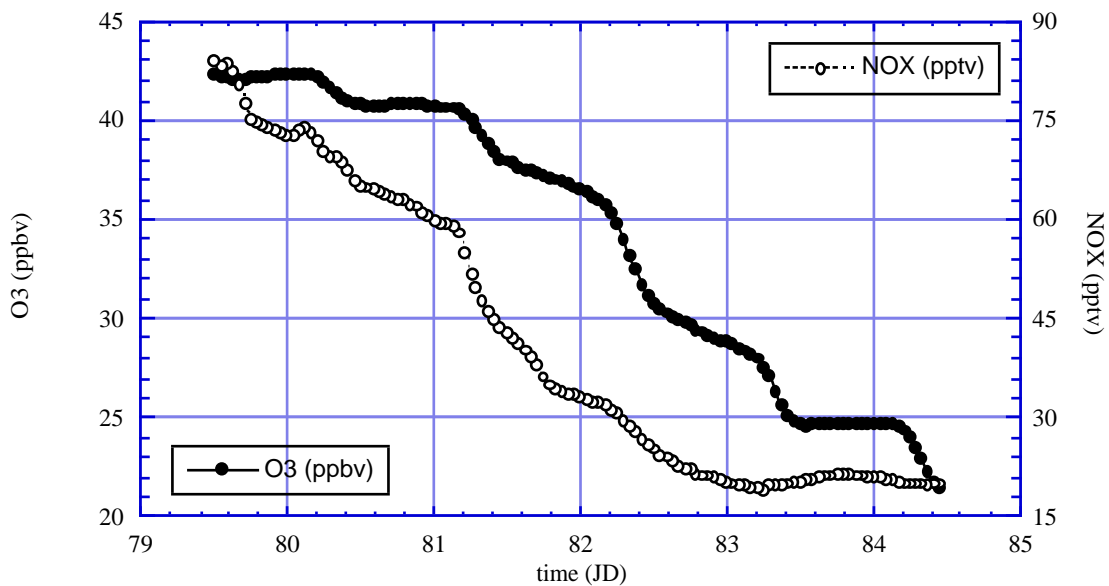
Figure 9d: O_3 and NO_x concentrations along back-trajectory B, as calculated with the ECHAM model.
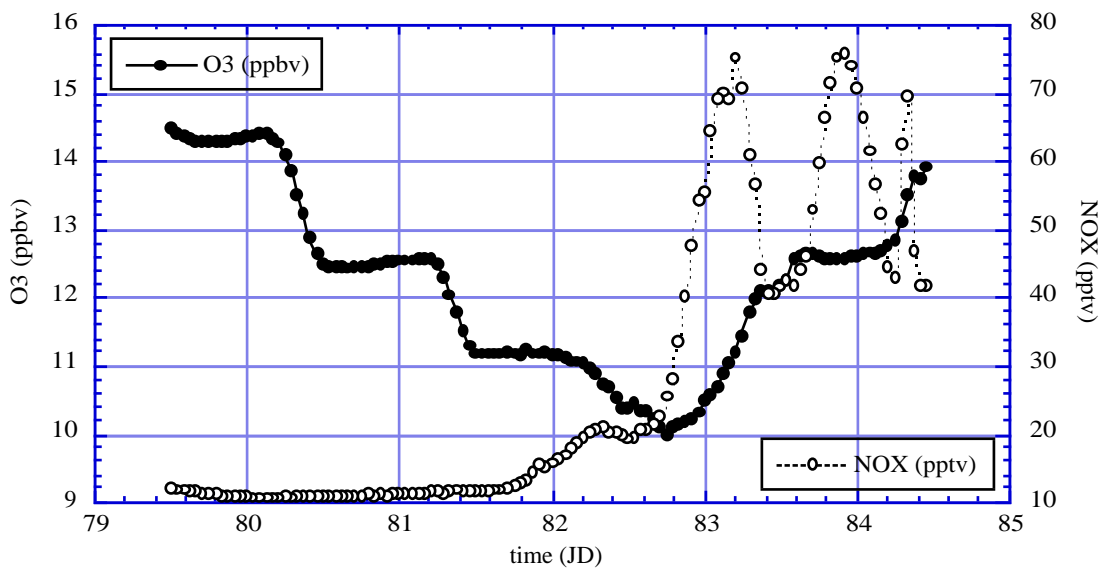

Figure 9e: As Figure 9d but for back-trajectory C.

Between JD 81.5 and 83.5 the daytime O_3 loss increases as NO_x is depleted to about 16-17 pptv. During this period the O_3 concentration also decreases during the night, caused by the reaction between O_3 and NO_2, heterogeneous removal of N_2O_5 and dry deposition of O_3 and HNO_3. An observer at a fixed point would see a relatively large amplitude in the diurnal O_3 cycle. Note that much of the variability in NO_x removal and net O_3

destruction is associated with (broken) clouds fields that (enhance) reduce photodissociation frequencies.

Figure 9e shows the NO_x concentrations along trajectory C. In this case the airmass moved from the Arabian Sea towards and along the African east coast. During the first three days the air is still moving away from the Indian O_3 source region. NO_x concentrations are low throughout the first three days, and O_3 shows the typical step-wise decrease. After JD 82 the airmass approaches the African coast and mixes with more polluted air. NO_x concentrations increase rapidly, and O_3 increases due to advection and local photochemical formation.

3.6   Summary and discussion

The model calculations show that the combination of horizontal advection, daytime net photochemical O_3 destruction and horizontal mixing cause a distinct diurnal O_3 cycle in the tropical MBL. The mechanisms can be summarized as follows:

1.   If NO_x concentrations exceed 50-100 pptv, net photochemical O_3 formation takes place, and the diurnal O_3 cycle shows a minimum at the end of the night and a maximum during late afternoon. This agrees, for example, with observations at Cape Grim (Tasmania) by Ayers *et al.* (1997), whose measurements were partially performed in relatively polluted air that was transported towards Cape Grim from the Australian continent.

2.   If O_3 and NO_x concentrations are still relatively high, but NO_x concentrations attain the net photochemical O_3 production regime, O_3 concentrations show a decrease during daytime, whereas during nighttime additional O_3 depletion can occur due heterogeneous removal of O_3 and NO_2 through N_2O_5. This also means that, due to the stronger horizontal O_3 gradient, the amplitude of the observed diurnal O_3 cycle is relatively large. This agrees with observations by Anderson *et al.* [1993] close to the polluted Brazilian coast, who measured amplitudes in the diurnal cycle between 2.75 and 4 ppbv (associated with a net O_3 destruction rate of about 8 ppbv day^{-1}). The measurements were performed in airmasses affected by biomass burning emissions of O_3 precursors (O_3 concentrations between 30 and 70 ppbv), thus showing large amplitudes in the diurnal O_3 cycle. The other campaigns listed in Table 2 indicate smaller diurnal O_3 cycles because the measurements were performed remote from pollution sources.

3.   If both NO_x and O_3 concentrations are relatively low, which is the case for much of the MBL, net photochemical O_3 destruction prevails during daytime. The diurnal O_3 cycle is also related to the intensity of sunlight. Oltmans [1981] showed that in Barrow, northern Canada (~ 70ºN), the diurnal O_3 cycle is much smaller than at Samoa (14ºS), associated with the much lower insolation at Barrow. Ayers *et al.* [1997] showed that at Cape Grim (41ºS) the diurnal O_3 cycle in summer is much larger than in winter. Our hypothesis implicates that a possible difference between the summer and wintertime boundary layer entrainment flux of O_3, as suggested by Ayers *et al.* [1997], is not necessary to explain the observed diurnal O_3 cycles.

Anderson *et al.* [1993] showed that, on average, the nighttime concentrations of O_3 in the boundary layer are higher than the daytime concentrations, and that the differences

are uniformly distributed over the entire boundary layer. This is an important observation because Vilà-Guerau de Arellano and Duynkerke [1999] demonstrated that, if chemical species are entrained from the free troposphere, the concentration differences in time should be higher close to the top of the boundary layer than close to the surface.

To further illustrate the different regimes, Figure 10 shows a global view of the diurnal O_3 cycle amplitude at the surface for the latter half of March, derived from the ECHAM model. The amplitude appears to be much larger and much more variable in the continental boundary layer (not shown) than in the MBL. This is related to the larger NO_x concentrations over land, which causes net O_3 production during daytime. The amplitude of the diurnal O_3 cycle over the ocean does not show such high variability, in line with the findings from the different campaigns listed in Table 2. Furthermore, over the oceans as well as over land the maximum amplitudes occur in areas with the highest insolation. These "bands" stretch zonally between 20ºN and 20ºS. The maximum amplitudes of the diurnal O_3 cycle in the MBL appear in areas where the average wind direction is offshore, e.g. the Indian west-coast, the Australian and Indonesian west coasts, the African west-coast and the west-coasts of central and southern America. This is related to the relatively high O_3 concentrations in net O_3 destruction environments. Figure 11 shows that the largest gradients in O_3 concentration gradients are found in a longitudinal band between the Equator and 15ºN, which is also the area where the largest diurnal O_3 cycle amplitudes occur. In the ITCZ over the Indian and Pacific Oceans, where O_3 concentrations reach minimum values, the diurnal O_3 cycle shows the smallest amplitude. Over the tropical Atlantic Ocean the O_3 concentrations do not reach values as low as those over the Indian and Pacific Oceans. Figure 12 shows the local time of the maximum in the diurnal O_3 cycle for the same period, as simulated by the ECHAM model. The marine regions show a maximum around sunrise, typical for net O_3 destruction regimes, and the local time of the maximum is very uniformly distributed. Over landmasses the maximum occurs during the day and over a wider range of local times, although always during daytime, which is typical for net O_3 production regimes.

This conceptual mechanism has several other implications. It explains the diurnal cycle for species, which have a relatively long lifetime (more than a few days) and which do not have an oceanic source. However, it does not describe the diurnal cycle of species with an oceanic source and/or very short lifetimes. This mechanism also implies that the often observed very low O_3 concentrations (< 5 ppbv) over marine regions, especially over the Pacific Ocean [Routhier *et al.*, 1980; Johnson *et al.*, 1990; Thompson *et al.*, 1993; Kley *et al.*, 1996], can be the result of airmasses having traveled and aged without interaction with more polluted airmasses from either the continents or from the free troposphere.

Although we propose that the entrainment process is not the main mechanism responsible for the observed diurnal cycle in O_3, entrainment of free tropospheric air into the boundary layer will have additional effects. The exact contribution of entrainment is, however, strongly dependent on the local conditions, for example the strength of the inversion and the O_3 concentrations in the free troposphere. Some observations of entrainment velocities in stratocumulus show an increase [de Roode and Duynkerke, 1997]. Other observations, however, do not show such an increase at all [Kawa and Pearson, 1989]. In general, the range of observed entrainment velocities is large and the methodologies used are associated with uncertainties. It also needs to be mentioned that
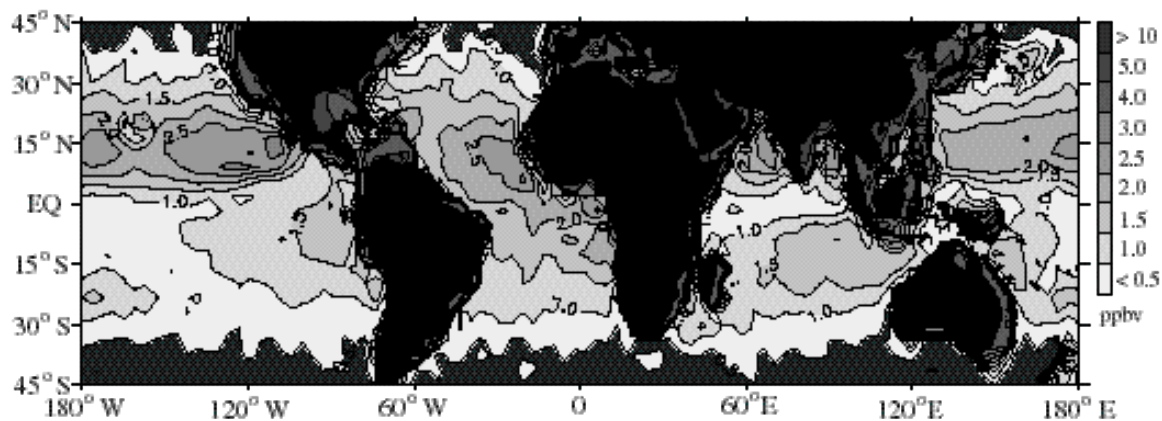
Figure 10: The average amplitude of the diurnal O_3 cycle at the surface over the globe, calculated by the ECHAM model for the period of 17 – 31 March 1995.
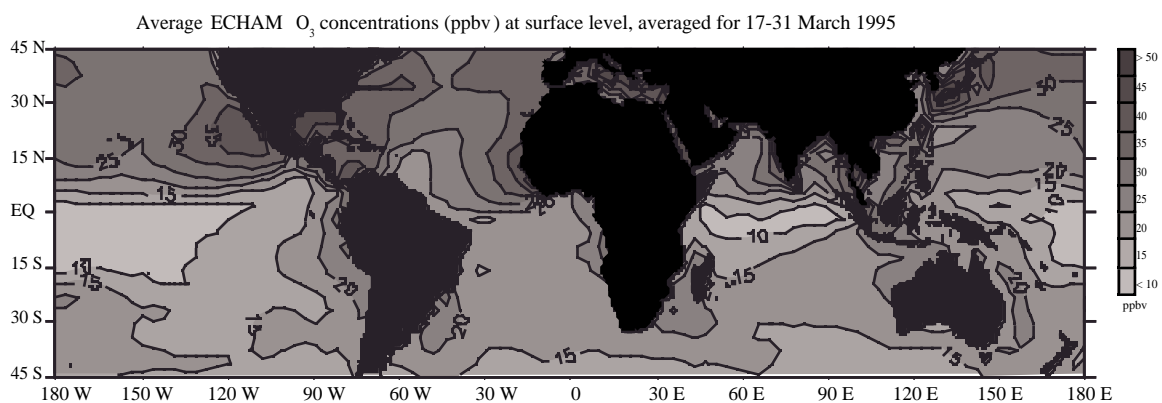

Figure 11: The average O_3 concentration at the surface over the globe from the ECHAM model, averaged for the period of 17-31 March 1995. For convenience the O_3 concentrations over landmasses have not been included.
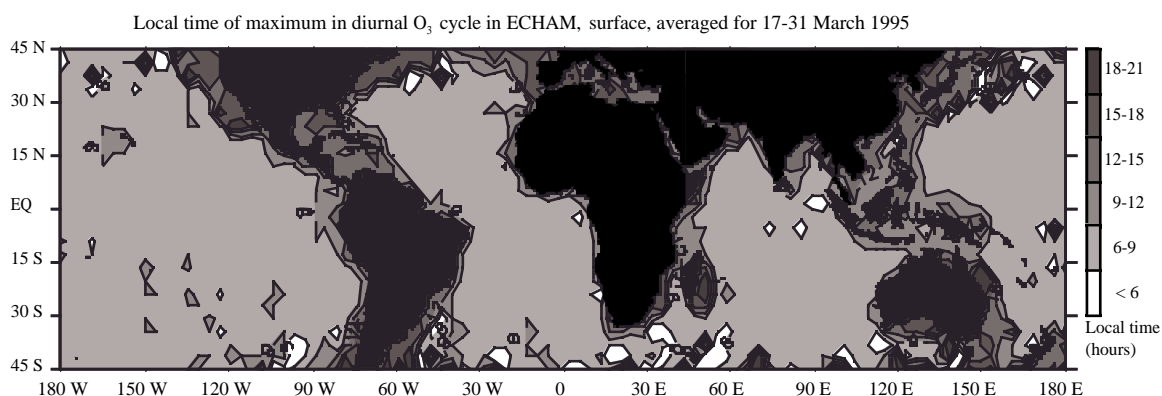

Figure 12: The local time at which the maximum amplitude in the diurnal cycle in O_3 appeared in the ECHAM model between 45ºN and 45ºS, averaged for the period of 17-31 March 1995.

entrainment in stratocumulus can lead to the breakup of the cloud layer [Duynkerke, 1993], after which entrainment velocities decrease.

3.7 Conclusions

It is shown that horizontal transport and photochemical processes explain the typical diurnal O_3 cycle in the MBL (nighttime maximum and daytime minimum). In this mechanism the daytime decrease and nighttime increase are closely related. Daytime net photochemical O_3 destruction in combination with horizontal advection and diffusion (due to turbulence) creates a gradual decrease (gradient) in O_3 from the source regions. Such a gradual decrease has been observed regulary, for example, over the Pacific and Indian Oceans [Johnson *et al.*, 1993; Lal *et al.*, 1998]. This gradient causes the nighttime increase because air with higher O_3 concentrations is advected to regions with lower O_3 concentrations. In this approach the daytime decrease will always be counteracted by the nighttime increase. The daytime depletion rate is thus a measure for the amplitude of the diurnal O_3 cycle. Although the horizontal advection of airmasses with higher O_3 concentrations continues during daytime, net photochemical O_3 destruction dominates the daytime O_3 tendency. As the daytime depletion is controlled by insolation, the amplitude of the diurnal O_3 cycle is very similar in most tropical marine regions. This is confirmed by the available observations (Table 2). This mechanism also implies that the amplitude of the diurnal O_3 cycle is larger close to NO_x emission regions because the O_3 concentrations are higher and net photochemical loss takes place at a higher rate, which is also in agreement with observations [Anderson *et al.*, 1993].

Finally we note that for MBL simulations of O_3 with a box model it is not relevant whether the mechanism that causes the diurnal O_3 cycle is entrainment of free tropospheric air (often assumed previously) or horizontal advection in conditions with photochemical O_3 loss (posed here). Both approaches have the same result: O_3 is transported from an area with higher O_3 concentrations Conclusion from studies in which box models have been used to explain the chemistry in the MBL are therefore not less valid, however, the physical mechanism behind the O_3 influx is different.